Cancer Cell International

RESEARCH

Open Access

Ailanthone disturbs cross-talk between cancer cells and tumor-associated macrophages via HIF1-α/LINC01956/FUS/β-catenin signaling pathway in glioblastoma

Xubin Deng[1†], Qianbing Zhang[2†], Fa Jin[3,4], Fengfei Lu[3,4], Guosheng Duan[5], Luwei Han[5], Meiling Zhu[5], Zhengyan Yang[5] and Gong Zhang[5*]

Abstract

Background An increasing number of studies have focused on ailanthone (aila) due to its antitumor activity. However, the role of ailanthone in glioblastoma(GBM) has not been investigated before. This study aims to explore the biological function and the underlying mechanism of ailanthone in GBM.

Methods The microarray analysis was used to screen out down-stream long non-coding RNAs (lncRNAs) targeted by ailanthone. Real-time PCR(RT-PCR) assay was used to examine LINC01956 expression levels. Colony-formation, Methylthiazolyldiphenyl-tetrazolium bromide(MTT), cell-cycle, organoids culture and in-vivo tumorigenesis assays were used to examine cell growth in vitro and in vivo. Boyden assay was used to examine cell invasion ability in vitro. RNA immunoprecipitation and RNA-protein pull-down assays were used to examine the interaction between LINC01956 and FUS protein. Chromatin Immunoprecipitation(ChIP) assay was used to examine HIF1-α-binding sites in the LINC01956 promoter.

Results Ailanthone decreased GBM cell growth in vitro and in vivo via inducing ferroptosis. Ailanthone treatment exhibited blood–brain barrier(BBB) permeability and specifically targeted the tumor area. LINC01956 was identified as a down-stream target of Ailanthone. LINC01956 exerted as an onco-lncRNA in GBM. M2 polarization of macrophages induced by exosomes derived from glioma cells overexpressing LINC01956 accelerated GBM progression. Mechanistically, we found that LINC01956 bound to FUS and reduced its ubiquitination. LINC01956 evoked nuclear translocation of phosphorylated (p)-β-catenin by recruiting FUS. Furthermore, under hypoxic conditions, LINC01956 was regulated by HIF-1α. Ailanthone decreased the expression of LINC01956 via suppressing HIF-1α.

Conclusion Taken together, our data revealed for the first time that ailanthone regulated HIF-1α/LINC01956/FUS/β-catenin signaling pathway and thereby inhibited GBM progression.

Keywords Ailanthone, FUS, GBM, HIF-1α, LINC01956, Tumor-associated macrophage

†Xubin Deng and Qianbing Zhang contributed equally to this work.

*Correspondence:
Gong Zhang
zhanggong7446@sxmu.edu.cn

Full list of author information is available at the end of the article

Introduction

High-grade glioma, also called glioblastoma (GBM), is a kind of brain cancer characterized by diffuse invasion and resistance to treatment [1]. Currently, a combination of neurosurgery, radiotherapy and chemotherapy is a common treatment for GBM patients. However, glioblastoma patients usually have a poor prognosis, with a 5-year survival rate of less than 5% [2]. Despite various therapeutic interventions being developed to tackle GBM, the overall survival rate remains disappointingly low. Thus, the urgent need to discover effective therapeutics capable of improving the prognosis for GBM patients is undeniable.

Long noncoding RNAs (lncRNAs), defined as noncoding transcripts > 200 nucleotides in length, are involved in diverse biological processes [3]. Recent documents have demonstrated that dysregulation of lncRNAs is closely related to a variety of pathological conditions, including glioma [4].

Tumor-associated macrophages (TAMs) infiltrate most solid tumors, which leads to cancer progression [5]. TAMs are a subtype of pro-tumoral macrophages with transcriptional and phenotypic characteristics distinct from those of M1 and M2 macrophages [6]. Depending on the polarization state, macrophages can be converted into two main types, M1 and M2 [7]. Recently, it was reported that lncRNAs can affect the polarization of TAMs [8]. Our previous studies have demonstrated that Wnt/β-catenin signaling is involved in the initiation and progression of various cancers [9, 10]. Wnt ligands secreted by glioma cells can activate Wnt/β-catenin signaling in macrophages and thereby induce M2 macrophage polarization [11].

Traditional Chinese Medicine(TCM), widely used in cancer treatment for a long time, has shown significant improvements in therapeutic efficacy. Recently, documents have found that TCM can affect TAMs and thereby inhibits tumor progression [12]. The ailanthone is a main active compound extracted from the stem barks of Ailanthus altissima (Mill.) and possesses various beneficial properties such as anti-tumor. However, the role of ailanthone in GBM has not been investigated.

In the present study, we find that ailanthone exhibits remarkable anti-cancer effects against GBM. We observe that ailanthone is able to significantly decrease the expression of LINC01956(an onco-lncRNA) in GBM cells. This substantial decrease in LINC01956 expression played a crucial role in inhibiting GBM progression. We manage to identify the HIF-1α/LINC01956/FUS/β-catenin signaling pathway as the primary target through which ailanthone exerted its anti-cancer actions.

Materials and methods

Reagents, cell culture and sample collection

Ailanthone was purchased from Dasfbio (Nanjing, China). The concentrations of used Ailanthone in treating U87 and U251 were 0.42μmol and 0.57μmol, respectively, according to the IC50 of Ailanthone. GBM cell lines were purchased from the Chinese Academy of Science (Shanghai, China). Cells were maintained in DMEM supplemented with 10% fetal bovine serum (FBS) in a 37 °C, 5% CO_2 incubator.

GBM and normal brain tissue samples were obtained from patients at People's Hospital of Shanxi Province and Zhujiang Hospital. Written informed consent was obtained from all patients prior to the study. All experiments were performed in accordance with the approved guidelines of the Institutional Research Ethics Committee of People's Hospital of Shanxi Province and Southern Medical University.

Culture of organoids

The fresh glioma tissues were collected and cultured in advanced Dulbecco's modifed Eagle's medium (DMEM)/F12, which contained 1% penicillin streptomycin. Subsequently, the glioma tissues were diced into approximately 2–3-mm sections, followed by digested at 37 °C for 1 h by trypsin. Then the digested tissues were filtered via 70 μm filter and the suspension was centrifuged. The cell pellet was resuspended in Matrigel, followed by plated in prewarmed (37 °C) 24-well culture plates. The growth rate of organoids was monitored on the indicated times.

Organoid imaging and growth evaluation

Organoid images were taken weekly or biweekly using an Olympus CKX53 inverted cell culture microscope (Shinjuku, Tokyo, Japan) at magnifications of 4x, 10x, and 20x. Organoid growth was assessed using two images taken approximately 14 days into culture, prior to passaging. Growth was categorized into three groups: group '–' indicated no significant growth, group '+' represented one to five organoids per well, and group '++' denoted more than five organoids per well.

RT-PCR analysis

To carry out RT-PCR analysis, total RNA was isolated from GBM cells by using TRIzol reagent (Invitrogen). Subsequently, this RNA was transcribed into cDNA by using HiScript II Q-RT SuperMix. Primers used for LINC01956 were: forward 5'-GCCACGTTCATTGCAC AGTT-3',Reverse5'-TCACTTTGCACCACAATGCG-3'. Primers used for GAPDH were: forward 5'-GGAGCGA GATCCCTCCAAAAT-3',Reverse5'-GGCTGTTGTCAT ACTTCTCATGG-3'.

MTT assay

First, GBM cells were seeded in 96-well plates and allowed to grow for 36 h. Subsequently, the medium was aspirated, and MTT solution was added to each well. After 30 min, 150 μL of DMSO was added to each well, and the absorbance was read at an OD of 590 nm.

Colony formation assay

GBM cells were seeded into 6-well culture plates and allowed to grow for two weeks. Subsequently, these cells were washed with phosphate-buffered saline (PBS) and stained with Giemsa solution.

Lentivirus transfection

The lentiviral vectors for LINC01956 down-regulation with target sequence (5′-CACCGCACAGTTTCGATTTGTTTAGCGAACTAAACAAATCGAAACTGTGC-3′) were designed and synthesized. U87 and U251 cells were infected according to the manufacture's protocol. The lentiviral shRNA control plasmid was added with a scrambled control sequence (ACAGAAGCGATTGTTGATC), which was basically mismatched.

Western blot analysis

To extract protein, RIPA buffer was used to lyse GBM cells. Then, proteins were separated by SDS-PAGE and transferred to polyvinylidene fluoride (PVDF) membranes. Subsequently, membranes were blocked with 5% nonfat milk and incubated first with primary antibodies at 4 °C overnight and then with HRP-conjugated secondary antibodies at room temperature for 1 h. The primary antibodies used in the study were listed as followings: x-CT(abcam, Lot NO.ab307601), GPX4(abcam, Lot NO.ab125066), FTH(abcam, Lot NO.ab75972), TFRC(abcam, Lot NO.ab182793), cyclinD1(abcam, Lot NO. ab134175), CDK4(abcam, Lot NO. ab108357), E-cadherin(abcam, Lot NO. ab40772), FUS(abcam, Lot NO. ab243880), CD63(abcam, Lot NO. ab134045), HSP70(abcam, Lot NO. ab2787), HIF-1α(abcam, Lot NO. ab51608), GAPDH(abcam, Lot NO. ab8245), anti-HA tag(abcam, Lot NO. ab236632), anti-FLAG tag(abcam, Lot NO. ab205606), N-cadherin(Cell Signaling Technology, Lot NO. #13116), Vimentin(Cell Signaling Technology, Lot NO. #5741), phospho-β-Catenin(Cell Signaling Technology, Lot NO. #9561) and c-myc (Cell Signaling Technology, Lot NO. #13987). All the concentrations of the antibodies used in the study were 1:1000. The levels of all proteins were determined by using enhanced chemiluminescence reagents.

Chromatin immunoprecipitation (CHIP) assay

The ChIP assay was performed with a ChIP assay kit (Millipore, catalog: 17–371) as previously described [13]. Enrichment of DNA fragments at the putative HIF1-binding sites in the LINC01956 promoter was assessed by RT-PCR.

RNA-binding protein pulldown assay

The RNA-binding protein pulldown assay was performed with a Pierce™ Magnetic RNA-Protein Pull-Down Kit (Thermo Fisher Scientific, MA, USA). The probe targeting LINC01956 was obtained from RiboBio, Guangzhou, China. Protein was eluted from the beads and separated with SDS-PAGE. Subsequently, the protein bands on the gel were subjected to silver staining. Western blot analysis was used to identify the proteins.

RNA immunoprecipitation (RIP) assay

The RIP assay was performed with a Magna RIP™ RNA-Binding Protein Immunoprecipitation kit (Millipore, Billerica, MA). The primary antibody against FUS was purchased from Santa Cruz (CA, USA). RT-PCR analysis was used to identify coprecipitated RNAs.

Immunofluorescence (IF) staining

To carry out the IF assay, cells grown on sterile glass coverslips were fixed with 4% paraformaldehyde and permeabilized with Triton X-100. Cells were incubated first with primary antibodies and then with secondary antibodies. DAPI was used to counter stain nuclei. A Nikon eclipse Ti-E inverted fluorescence microscope was used to acquire images.

Biolayer interferometry (BLI)

An Octet system (ForteBio, Fremont, CA) was used to carry out BLI. Biotin-labeled LINC01956 was immobilized on a streptavidin sensor.

Coimmunoprecipitation (co-IP) assay

The interactions among LINC01956, FUS and β-catenin were validated by a co-IP assay that was described in a previous report [14].

Exosome isolation

To isolate exosomes, culture medium from glioma cells was centrifuged first at 500×g for 5 min and then at2000×g for 30 min. Subsequently, 2×PEG solution was mixed with the supernatant. Later, the mixture was centrifuged at 10,000×g for 1 h.

BBB permeability assay

Intracranial xenografts of U87 cells (1×10^6) in mice were administered ailanthone intravenously. Brain tumor and normal brain tissues were collected at various intervals post-injection.

ROS assay

The generation of reactive oxygen species (ROS) was assessed utilizing a ROS assay kit (catalog number). no.S0033S; Beijing Solarbio Science & Technology Co., Ltd.) following the manufacturer's protocol. GBM cells were cultured in 6-well plates and exposed to ailanthone for 24 h. Afterward, 10 μM DCFH-DA was introduced to each well and incubated in the dark for 20 min. The cells were washed three times with serum-free medium, digested, and then transferred to a 96-well plate at a consistent density. Fluorescence intensity was recorded using a BioTek Instruments microplate reader at 488 nm excitation and 525 nm emission wavelengths. Fluorescence was directly observed using a fluorescence microscope.

Identification of markers associated with ferroptosis

Intracellular concentrations of Fe^{2+}, lipid peroxidation (LPO), malondialdehyde (MDA), glutathione (GSH), and catalase (CAT) were measured using the Fe^{2+} assay kit. no.A039-2-1), LPO assay kit (cat.no.A106-1-1), MDA assay kit (cat.no.A003-1-1), GSH assay kit (cat.no.A061-1-2) and CAT assay kit (cat.no.A007-1-1), respectively, according to the manufacturer's protocols. The kits were sourced from Nanjing Jiancheng Bioengineering Institute.

TEM(transmission Electron microscope) assay

Transmission electron microscopy (TEM) was employed for the ultrastructural examination of mitochondria. Cells, either treated with ailanthone or left as controls, were exposed to 5 μM erastin or not, then fixed in 2.5% glutaraldehyde in 0.1 M PBS (pH 7.4) at 4 °C for 2.5 h. They were subsequently washed three times with 0.1 M PBS and postfixed in 1% OsO4 for 2 h at 4 °C. The samples were dehydrated using an ethanol gradient and embedded in Spurr's resin. Ultrathin sections were stained with uranyl acetate or lead citrate and analyzed using a JEOL 1200EX transmission electron microscope.

In vivo tumor growth experiment

The care of animals was carried out in accordance with the approved guidelines of the Institutional Research Ethics Committee of Shanxi Medical University and Southern Medical University. Luciferase-expressing sh-LINC01956 cells and sh-ctrl cells(1×10^6) were injected into the brain parenchyma of nude mice using a previously described protocol [15]. Glioma xenografts were monitored at 7 and 21 days after cell injection via an IVIS Spectrum Live Imaging System (Caliper Life Sciences, Mountain View, CA).

Results

Ailanthone inhibited GBM cell growth in vitro and in vivo

This study initially examined ailanthone's inhibitory impact on GBM cell growth. We first conducted ailanthone susceptibility tests on GBM cell lines(U87 and U251). The IC50 of ailanthone on U87 cell line was 0.42μmol, while on U251 cell line was 0.57μmol(Fig. 1A). Subsequently, we sought to determine whether ailanthone had an effect on cell growth in vivo. To this end, U87 and U251 were injected into the brains of nude mice to establish an orthotopic glioma xenograft model. We

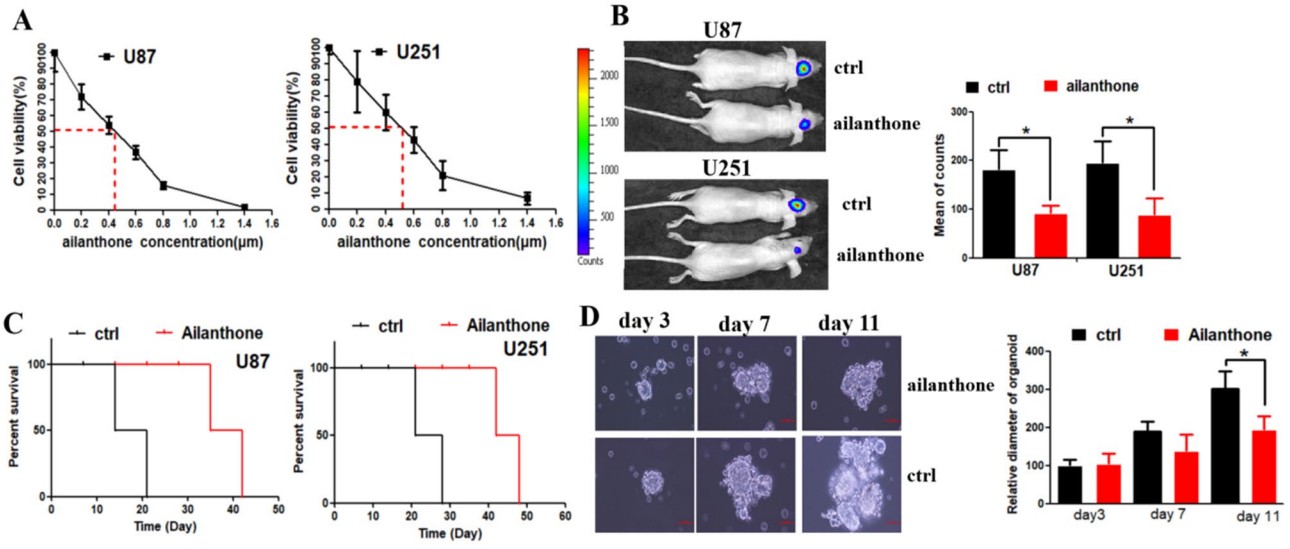

Fig. 1 Ailanthone inhibited GBM cell growth in vitro and in vivo. (**A**) GBM cell viability was analyzed via MTT assay. (**B**) PDX models were established with brain parenchyma inoculation of nude mice with U87 and U251 cell lines. Cell lines were pre-treated with DMSO(control group) or ailanthone. (**C**) GBM cells were implanted intracranially into nude mice. Mice were injected i.v. with control ($n=5$) or 150 ng/g ailanthone ($n=5$) daily, the Mantel–Cox log–rank test was used for analysis, and the relative survival curves are shown. (**D**) The patient-derived organoid (PDO) models were used to analyze ailanthone effect on GBM cells. *$p<0.05$. Data are presented as Mean ± SD. One way ANOVA. Log-rank test was used in Kaplan-Meier survival analysis

further verified the effect of ailanthone on GBM PDX models and found that it also had a good inhibitory effect in vivo(Fig. 1B). Interestingly, nude mice treated with ailanthone exhibited prolonged survival times when compared with the control group (Fig. 1C). In order to better simulate the anti-cancer effect of ailanthone in GBM, we established personalized patient-derived organoid (PDO) models to further investigate ailanthone's effect on GBM cells. As revealed in Fig. 1D, ailanthone treatment significantly suppressed the glioma cell growth in two PDO models.

Taken together, these data suggested that ailanthone inhibited GBM cell growth in vitro and in vivo.

Ailanthone promoted ferroptosis in GBM cells

The fast-growing studies of ferroptosis in cancer have boosted a perspective for its usage in cancer therapeutics. A recent report documented that ailanthone induced ferroptosis in non-small cell lung cancer lewis cells [16]. We then asked whether ailanthone inhibited GBM cell death by inducing ferroptosis. ROS accumulation is a key indicator of ferroptosis; thus, ROS levels in GBM cells exposed to varying concentrations of ailanthone were measured using the fluorescent dye DCFH-DA. The results obtained by fluorescence microscopy(Fig. 2A) and a fluorescent microplate reader (Fig. 2B) revealed that the red fluorescence intensity increased while treated by ailanthone. Ferroptosis is primarily characterized by iron overload and redox imbalance.The intracellular Fe^{2+} concentration was measured with an iron assay kit. As demonstrated in Fig. 2C, the intracellular Fe^{2+} content increased with treated with ailanthone.The impact of ailanthone on ferroptosis was examined by evaluating the intracellular redox state with reagent kits.The study found that ailanthone treatment led to increased concentrations of LPO (Fig. 2D) and MDA (Fig. 2E), whereas GSH (Fig. 2F) and CAT (Fig. 2G) levels decreased.

Furthermore, the protein levels of four genes related to ferroptosis(xCT, GPX4, FTH, and TFRC) were assessed. Western blot assay results revealed that ailanthone decreased the protein expression levels of xCT, GPX4 and FTH while increasing the protein expression level of TFRC in GBM cells (Fig. 2H). Taken together, these results demonstrated that ailanthone induced ferroptosis in GBM cells.Transmission electron microscopy (TEM) analysis further revealed that ailanthone-treated cells contained shrunken mitochondria with elevated membrane density, a typical morphologic feature of ferroptosis (Supplementary Fig. 1A).

Ailanthone treatment demonstrated blood-brain barrier permeability and selectively targeted the tumor region

We analyzed concentration of ailanthone in the tumor area by using intracranial xenograft mouse model. Interestingly, the concentration of ailanthone reached its peak just 10 min after intravenous injection of ailanthone, with a measured value at 108 ng/g of tissue. Notably, the concentration in the tumor area was found to be as least twice as high as that in the nontumor area, indicating that ailanthone specifically targets the tumor area (Fig. 2I).

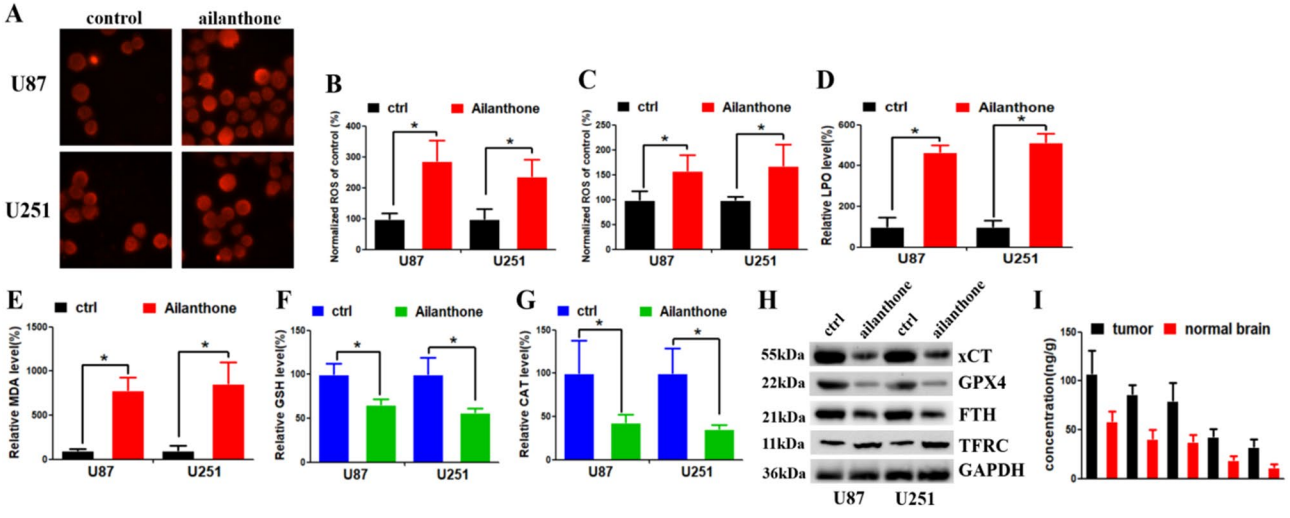

Fig. 2 Ailanthone promoted ferroptosis in GBM cells. (**A**) Relative fluorescence intensity of ROS in GBM cells treated by ailanthone under a fluorescence microscope. (**B**) Relative fluorescence levels of ROS in GBM cells treated by ailanthone, as detected by fluorescent enzyme label. (**C**)-(**G**) Colorimetry detection of the levels of Fe^{2+}, LPO, MDA, GSH and CAT in GBM cells treated with ailanthone. (**H**) Western blot analysis of ferroptosis-associated proteins xCT, GPX4, FTH and TFRC in GBM cells treated with ailanthone. (**I**) The ailanthone concentration in the tumor area and normal brain tissue following a single injection of ailanthone. *$p < 0.05$. Data are presented as Mean ± SD. One way ANOVA

Ailanthone inhibited LIN01956 expression levels in GBM cells

Previous studies have revealed that lncRNAs are involved in the progression of GBM cells, so we hypothesized that some lncRNAs might take part in the ailanthone treatment. We used Arraystar Human lncRNA array to find the lncRNAs that may be regulated by ailanthone. It was found that ailanthone can regulate the expression of a series of lncRNAs, among which LIN01956 had a more pronounced response to ailanthone (Fig. 3A). To better understand the clinical relevance of these identified LncRNAs, we analyzed their impact on patient survival

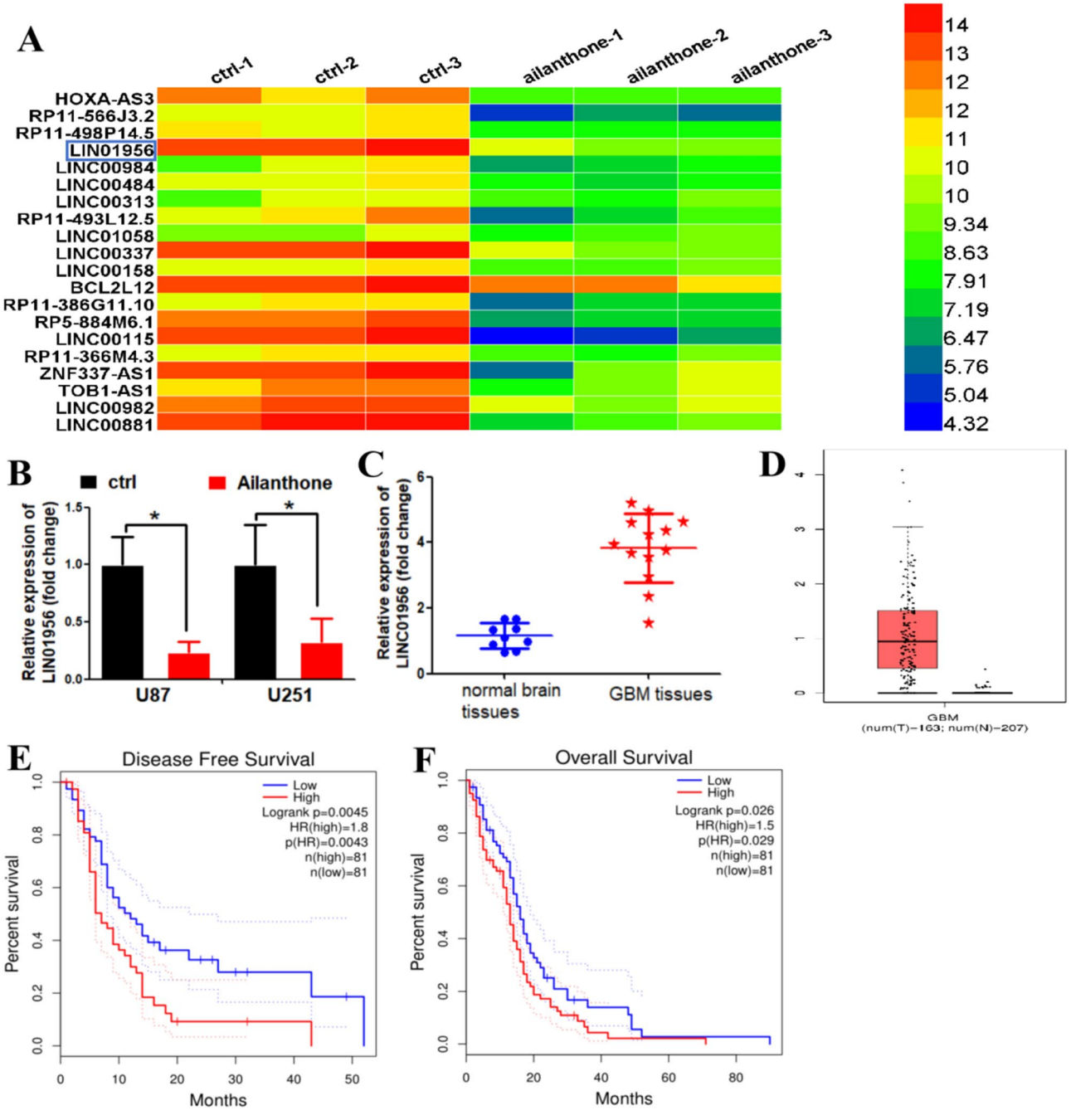

Fig. 3 Ailanthone inhibited LIN01956 expression levels and the expression level of LINC01956 was associated with poor clinical outcome in GBM. (**A**)-(**B**) Ailanthone inhibited LIN01956 expression, as revealed by Arraystar Human lncRNA array and RT-PCR, respectively. (**C**) RT-PCR was used to examine LIN01956 expression in GBM and normal brain tissues. (**D**) GEPIA database was used to analyze LIN01956 expression level in GBM and normal brain tissues. (**E**)-(**F**) The association between expression level of LINC01956 and overall survival/disease-free survival was revealed by GEPIA database, respectively. *$p < 0.05$. Data are presented as Mean ± SD. One way ANOVA. Log-rank test was used in Kaplan-Meier survival analysis

using GEPIA (Gene Expression Profiling Interactive Analysis) (http://gepia.cancer-pku.cn/), a widely-used tool that integrates data from the TCGA databases. LIN01956, a lncRNA which was highly associated with GBM patients, caught our attention.

We then used RT-PCR assay to examine ailanthone's effect on LIN01956 expression. It was found that ailanthone treatment decreased LIN01956 expression level in both U87 and U251 cell lines(Fig. 3B).

The expression level of LINC01956 was elevated in GBM tissues and associated with poor clinical outcome

We then asked whether LINC01956 was involved in the progression of GBM. We found that the expression level of LINC01956 was elevated in glioma tissues compared with normal brain tissues (Fig. 3C). This finding was also confirmed by using the GEPIA server (http://gepia.cancer-pku.cn/, which analyzes data from TCGA and GTeX, Fig. 3D). In addition, GBM patients with a high expression level of LINC01956 tended to have poorer overall survival and disease-free survival rates than those with low expression levels of LINC01956 (Fig. 3E and F, data analyzed with GEPIA). The time ROC analysis was carried out to compare the predictive accuracy and risk score of LINC01956 for OS and DFS in glioma by using the TCGA database. In the OS analysis, LINC01956 expression level could predict the prognosis of glioma patients at 1, 3 and 5 years, and its AUC under the ROC curve was 0.75, 0.808 and 0.725, respectively (Supplementary Fig. 1B). In the DFS analysis, AUC under the ROC curve was 0.75, 0.805 and 0.734, respectively (Supplementary Fig. 1C). These data fully implicated that LINC01956 could be an ideal marker for predication of OS and DFS in glioma.

Correlation of LINC01956 expression levels with clinicopathological features in glioma

We then analyzed the correlation of LINC01956 expression levels with clinicopathological features in glioma by mining the data from TCGA. It was found that LINC01956 expression levels increased gradually with the glioma WHO grades. Glioma patients with WHO grade 4 had the highest expression level of LINC01956 than other patients (Supplementary Fig. 1D). In addition, LINC01956 expression level was highly expressed in glioblastoma patients, when compared with that in other histological types (Supplementary Fig. 1E). We also found that LINC01956 expression level was decreased in IDH mutant patients when compared with that in IDH wild type patients (Supplementary Fig. 1F). Interestingly, LINC01956 expression level was significantly associated with patient treatment outcome. In glioma patients with poor outcome(progressive disease), the LINC01956 expression level was significantly higher than that in those patients with clinical benefit (complete response, partial response and stable disease) (Supplementary Fig. 1G). In the univariate analysis, WHO grade, 1p/19q codeletion, IDH status, histological type andLINC01956 expression level affected the prognosis of glioma patients (all $p<0.05$).Furthermore, multivariate cox regression showed that the above characteristics were also independent risk factors for unfavorable OS of glioma (Table 1).

LINC01956 inhibition decreased GBM cell growth and invasion

Firstly, genes coexpressed with LINC01956 (|logFC|>1, P.adj<0.05) were selected to perform gene enrichment analysis, followed by GO term analysis. The biological process (BP) analysis showed positive regulation of cell cycle process, positive regulation of cell cycle phase

Table 1 Univariate and multivariate analysis of clinicopathological factors that correlate with OS of glioma patients

Characteristics	Total(*N*)	Univariate analysis		Multivariate analysis	
		Hazard ratio (95% CI)	*P* value	Hazard ratio (95% CI)	*P* value
WHO grade	634				
G2	223				
G3&G4	411	5.642 (3.926–8.109)	**< 0.001**	1.842 (1.203–2.822)	**0.005**
1p/19q codeletion	688				
codel	170				
non-codel	518	4.428 (2.885–6.799)	**< 0.001**	1.796 (1.075-3.000)	**0.025**
IDH status	685				
WT	246				
Mut	439	0.117 (0.090–0.152)	**< 0.001**	0.320 (0.219–0.468)	**< 0.001**
LINC01956	695				
Low	348				
High	347	3.648 (2.805–4.745)	**< 0.001**	2.120 (1.559–2.883)	**< 0.001**
Histological type	695				
Astrocytoma&Oligoastrocytoma&Oligodendroglioma	527				
Glioblastoma	168	9.114 (7.008–11.853)	**< 0.001**	2.733 (1.961–3.808)	**< 0.001**

transition, epithelial cell proliferation and positive regulation of cell−cell adhesion. The cellular component (CC) analysis showed that spindle, spindle microtubule and collagen-containing extracellular matrix were significantly enriched. The molecular fuction (MF) analysis showed that growth factor activity, chemokine activity, cytokine receptor binding and cytokine activity were significantly enriched. In the KEGG analysis, we found that cell cycle, cell adhesion molecules and focal adhesion were significantly enriched (Supplementary Fig. 2A). These data implicated that LINC01956 may participate in cell signaling functions that regulate proliferation and invasion of glioma.

Based on the above findings, we then performed biological function assay to analyze LINC01956's function on glioma cell proliferation and invasion. GBM cell lines (U87 and U251) were used in this functional study. First, we established cells in which LINC01956 was stably knocked down (sh-LINC01956) and a control cell group, namely, sh-ctrl (Fig. 4A). Cell growth was examined by MTT and colony formation assays. As revealed by the MTT assay, LINC01956 downregulation decreased cell viability (Fig. 4B). In parallel, the colony formation assay revealed that sh-LINC01956 cells formed smaller and fewer colonies than sh-ctrl cells (Fig. 4C, Supplementary Fig. 2B). We further sought to determine whether LINC01956 affects the cell cycle distribution. The frequency of GBM cells in G1 phase was significantly higher than that in S phase when LINC01956 was knocked down, as revealed by flow cytometric analysis (Fig. 4D, Supplementary Fig. 2C). In parallel, G1/S cell cycle checkpoint proteins (e.g., cyclinD1 and CDK4) were downregulated in sh-LINC01956 cells (Fig. 4E). Together, these findings imply that LINC01956 promotes the transition from G1 to S phase and thus promotes GBM cell growth in vitro. The Boyden chamber assay showed that LINC01956 inhibition decreased the invasion ability of GBM cells(Fig. 4F, Supplementary Fig. 2D). Subsequently, we analyzed the expression levels of epithelial-mesenchymal transition (EMT)-related proteins by western blot analysis. Interestingly, LINC01956 downregulation inhibited N-cadherin and vimentin expression and elevated E-cadherin expression levels (Fig. 4G). These data suggested that downregulation of LINC01956 reversed the EMT phenotype.

Subsequently, we sought to determine whether LINC01956 has an effect on cell growth in vivo. To this end, luciferase-expressing U87 cells transduced with sh-ctrl or sh-LINC01956 were injected into the brains of nude mice to establish an orthotopic glioma xenograft model. We observed that the growth of sh-LINC01956-transduced cells was significantly slower than that of

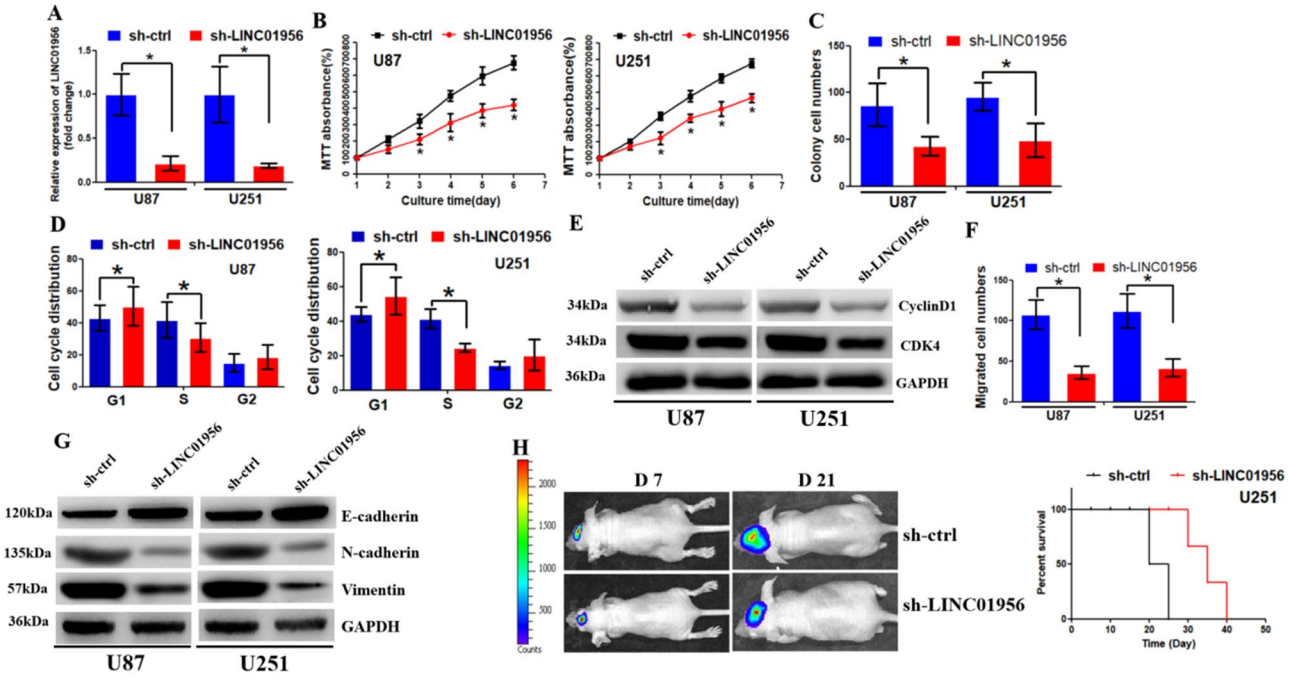

Fig. 4 LINC01956 inhibition decreased GBM cell growth and invasion. (**A**) RT-PCR assay was used to examine LINC01956 expression levels in sh-ctrl and sh-LINC01956 cells, respectively. (**B**) MTT assay was used to examine cell viability. (**C**) The colony formation assay was used to measure cell colony formation ability. (**D**) The flow cytometry assay was used to examine cell cycle distribution. (**E**) Western blot assay was used to examine protein expression levels. (**F**) Boyden assay was used to test cell invasion ability. (**G**) Western blot assay was used to examine expression levels of E-cadherin, N-cadherin and Vimentin. (**H**) An orthotopic glioma xenograft model was established to monitor LINC01956's effect on cell growth in vivo, and the relative survival curves are shown. *$p < 0.05$. Data are presented as Mean ± SD. One way ANOVA.Log-rank test was used in Kaplan-Meier survival analysis

sh-ctrl-transduced cells (Fig. 4H). These findings indicate that downregulation of LINC01956 inhibits tumorigenesis of glioma cells in vivo.

LINC01956 promoted GBM cell progression via the WNT/β-catenin signaling pathway

We next performed RNA sequencing to examine the difference in transcript expression levels between sh-ctrl and sh-LINC01956 cells (fold change>2, supplementary Table 1). Gene ontology analysis, KEGG pathway enrichment and Gene Set Enrichment Analysis (GSEA) analysis revealed that the WNT/β-catenin pathway was significantly altered when LINC01956 was downregulated (Supplementary Fig. 3A-B). Western blot analysis revealed that downregulation of LINC01956 decreased the levels of phosphorylated β-catenin and its downstream targets (c-myc and cyclinD1, Fig. 5A). The immunofluorescence assay revealed that downregulation of LINC01956 impaired the translocation of β-catenin into the nucleus (Fig. 5B, supplementary Fig. 3C). In addition, downregulation of LINC01956 markedly decreased TOP/FOP transcriptional activity (Fig. 5C). These data suggest that downregulation of LINC01956 suppresses WNT/β-catenin signaling pathway activity.

To examine whether the WNT/β-catenin pathway mediates the effect of LINC01956 on GBM cell progression, we used LiCl(a key activator of the WNT/β-catenin pathway) to perform rescue experiments in LINC01956-silenced cells. As expected, the suppressive effect of LINC01956 downregulation on cell growth and invasion were significantly reduced in the context of LiCl addition (Fig. 5D-G). Collectively, our data suggest that the WNT/β-catenin pathway mediates the pro-motive effect of LINC01956 on GBM invasion.

LINC01956 bound to FUS and reduced its ubiquitination

RT-PCR showed that LINC01956 is localized in both the cytoplasm and the nucleus (Supplementary Fig. 4A). The starBase database (http://starbase.sysu.edu.cn/starbase2/rbpLncRNA.php) was used to identify interactions between LINC01956 and potential RNA-binding proteins (RBPs). Among these RBPs, we found that there were three RBPs (FUS, NOP56 and TIA1) that interacted with LINC01956 (Supplementary Fig. 4B). We focused on FUS because FUS participated in the regulation of GBM cell progression. We performed a series of experiments to confirm the association between LINC01956 and FUS. We used SDS-PAGE to isolate proteins complexes pulled down with a probe targeting LINC01956. Among the bands, that the band corresponding to FUS was present in the immune blot of the precipitate pulled down with the probe targeting LINC01956 and not in that pulled down with the control probe (Supplementary Fig. 4C). RNA pull-down and RIP assays revealed

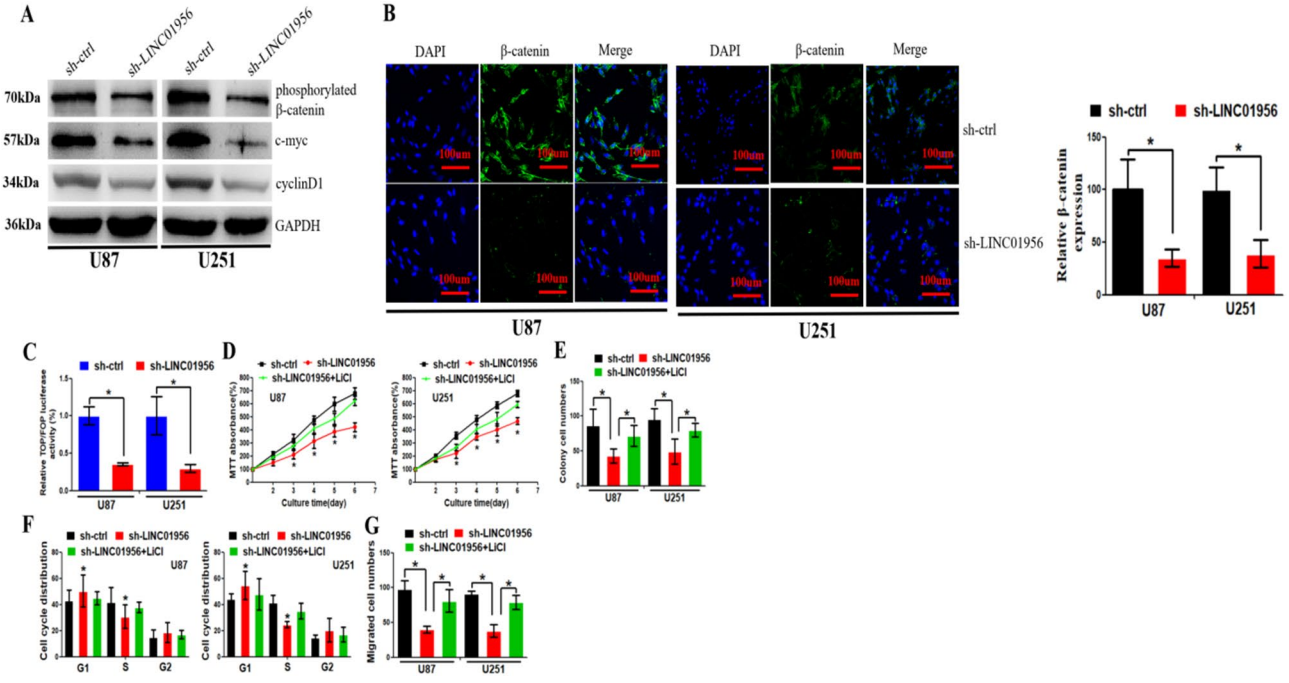

Fig. 5 LINC01956 promotes GBM cell progression via the WNT/β-catenin signaling pathway. (**A**) Western blot assay was used to examine protein expression levels. (**B**) The immunofluorescence assay was used to examine β-catenin cellular position. (**C**) TOP/FOP flash reporter assay was performed to examine β-catenin activity. (**D**) MTT assay was used to examine cell viability. (**E**) Colony formation assay was used to measure cell proliferative ability. (**F**) The flow cytometry assay was used to examine cell cycle distribution. (**G**) Boyden assay was used to test cell invasion ability.*$p < 0.05$. Data are presented as Mean ± SD. One way ANOVA

that LINC01956 directly interacted with FUS in U87 and U251 cells (Fig. 6A). Furthermore, we used a series of LINC01956 deletion mutants to map the FUS binding region. We found that LINC01956 mutant Δ3 bound to FUS as efficiently as full-length LINC01956, whereas the binding capacity of the other mutants was completely abolished (Fig. 6B). Via an immunofluorescence assay, we identified colocalization of LINC01956 and FUS in GBM cells (Fig. 6C).We then demonstrated that the total protein level of FUS was decreased by LINC01956 inhibition, while its mRNA level was not altered (Fig. 6D). Subsequently, a cycloheximide (CHX) chase assay was performed to examine whether LINC01956 can maintain FUS protein stability. The half-life of the FUS protein was significantly decreased to approximately 16 h in cells with LINC01956 downregulation, whereas it was greater than 24 h in the control group, as revealed by western blot analysis (Fig. 6E). The ubiquitination assay revealed a significant increase in polyubiquitinated FUS protein in cells with LINC01956 downregulation (Fig. 6F).

Taken together, these data suggest that LINC01956 binds to FUS and reduces its ubiquitination.

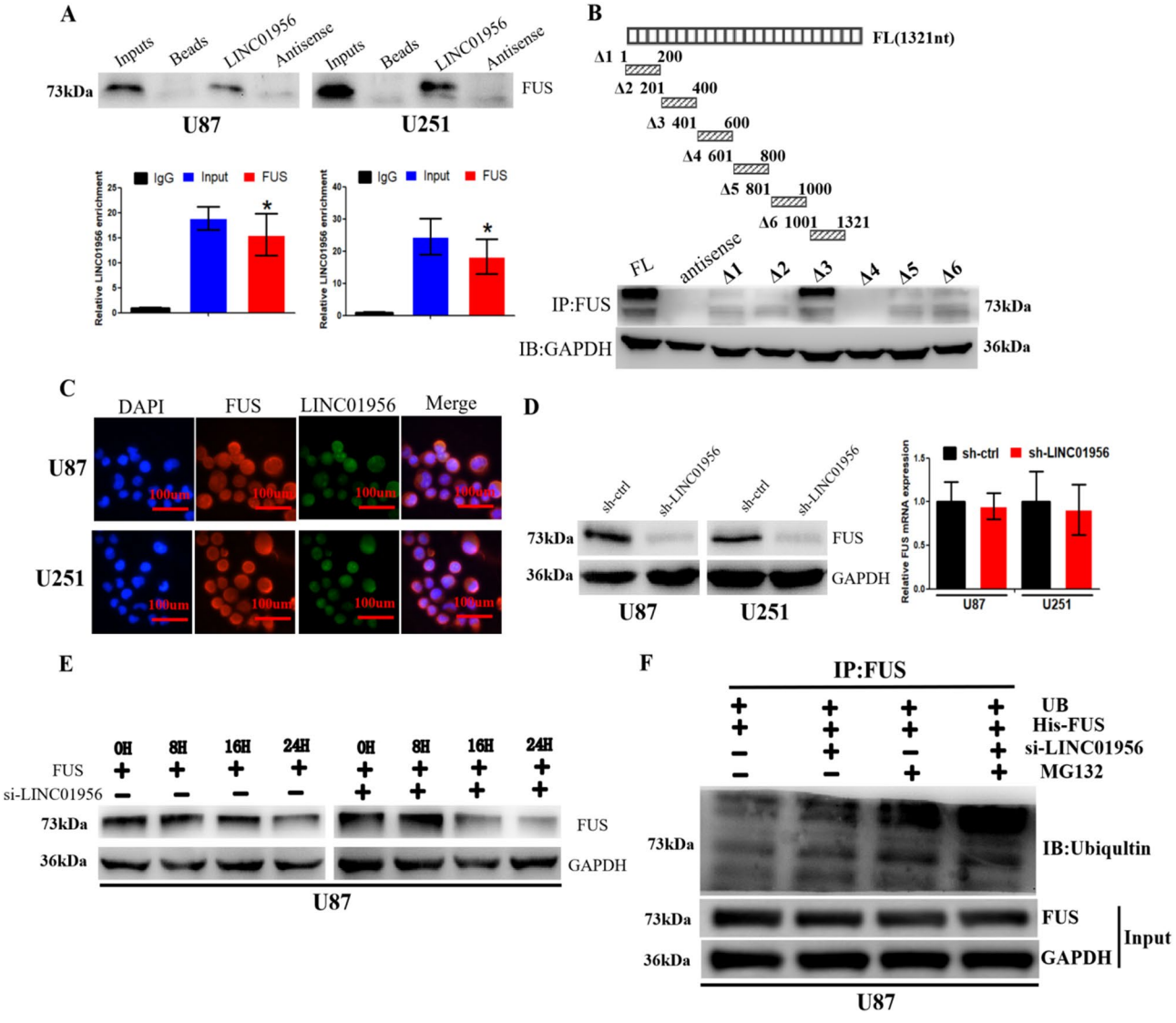

Fig. 6 LINC01956 bound to FUS and reduced its ubiquitination. (**A**) The RNA pull-down and RIP assays were performed to examine interaction between LINC01956 and FUS. (**B**) Bio-layer interferometry (BLI) analysis of biotinylated-LINC01956 binding to FUS protein. (**C**) The immunofluorescence assay was used to examine cellular location of LINC01956 and FUS. (**D**) Down-regulation of LINC01956 decreased FUS protein expression level(left panel). Down-regulation of LINC01956 did not affect FUS mRNA expression level(right panel). (**E**) Cycloheximide (CHX) chase assay combined with western blot assay were used to examine FUS protein stability. (**F**) Western blot assay was used to analyze ubiquitination of FUS protein. *$p < 0.05$. Data are presented as Mean ± SD. One way ANOVA

LINC01956 facilitated the translocation of β-catenin into the nucleus of GBM cells by recruiting FUS

The interaction between FUS and β-catenin was predicted by starBase (Supplementary Fig. 4D). The co-IP assay was performed to confirm the interaction between FUS and β-catenin. The co-IP assay revealed that tagged HA-β-catenin and FLAG-FUS coprecipitated with LINC01956-FLAG but not with immunoglobulin G (IgG) (Fig. 7A). These data suggest that β-catenin, FUS and LINC01956 form a complex. In addition, we observed that overexpression of FUS counteracted the decrease in the level of nuclear phosphorylated (p)β-catenin in sh-LINC01956 GBM cells (Fig. 7B). In parallel, the immunofluorescence assay revealed that downregulation of LINC01956 inhibited nuclear translocation of β-catenin and that this effect was abrogated in the context of FUS cotransfection (Fig. 7C). Taken together, we speculate that LINC01956 leads to nuclear translocation of activated β-catenin in cooperation with FUS.

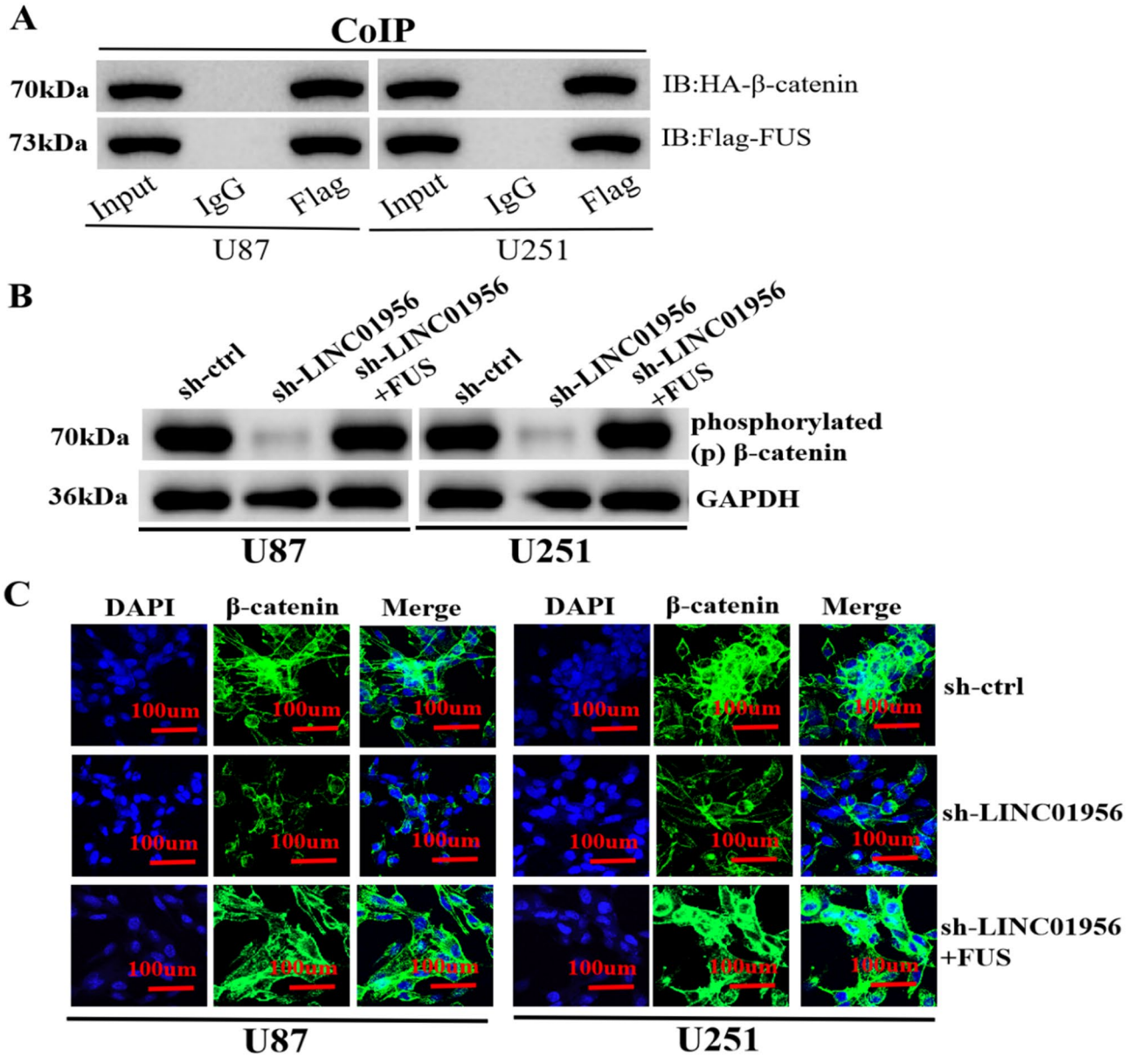

Fig. 7 LINC01956 facilitated the translocation of β-catenin into the nucleus of GBM cells through recruiting FUS. (**A**) The existence of the complex containing LINC01956, FUS, and β-catenin was validated using coIP assay. (**B**) Western blot assay was used to examine protein expression levels. (**C**) The immunofluorescence assay indicated that down-regulation of LINC01956 inhibited nuclear translocation of β-catenin, which was abrogated in the context of FUS con-transfection

Exosomal LINC01956 promoted M2 polarization of macrophages

The tumor-infiltrating lymphocytes may affect prognosis of various of cancer, including glioma. We then explored the association between LINC01956 and 24 immune-cell subsets in glioma by means of ssGSEA with Spearman r. The data were present in supplementary Fig. 3D. Among the analysis, the significant correlation between LINC01956 and infiltration levels of macrophages caught our attention. Because activation of the Wnt/β-catenin pathway contributes to M2 polarization; we thus sought to determine whether LINC01956 affectsM2 polarization. To this end, we evaluated the expression levels of LINC01956, M1 markers, and M2 markers in unpolarized macrophages, LPS/INF-γ-induced M1 macrophages, and IL-4/IL-13-induced M2 macrophages. We observed elevated expression of M1-associated genes (CD80, MCP-1 and iNOS) in M1 macrophages and of M2-associated genes (CD206 and MRC-2) in M2 macrophages (Fig. 8A). This result indicated the successful polarization of macrophages. Compared with that in M1 macrophages, the expression level of LINC01956 in M2 macrophages was elevated (Fig. 8B). These data suggest that LINC01956is involved in macrophage polarization. Subsequently, we treated THP-1 cells with PMA for 24 h, transfected them with si-ctrl or si-LINC01956 and added IL-4 and IL-13 to induce polarization toward the M2 phenotype. In si-LINC01956 cells, the levels of M1 markers were markedly increased, and the levels of M2 markers were significantly decreased (Fig. 8C). In contrast, LINC01956 overexpression led to the opposite result(Fig. 8D). In addition, when compared with supernatant from control cells, supernatant from pcDNA-LINC01956 cells led to increased expression of M2 markers (Fig. 8E).

Subsequently, we explored the interactions between GBM cells and macrophages. Previous studies demonstrated that lncRNAs can be transferred by exosomes and thereby regulate the tumor microenvironment (TME) [17]. We hypothesized that LINC01956 may be transferred in this way. We isolated exosomes from the supernatants of cultured GBM cells and measured the levels of the exosome-related proteins CD63, HSP70, and HSP90 by western blot analysis (Fig. 8F). Downregulation of LINC01956 led to decreased levels of LINC01956

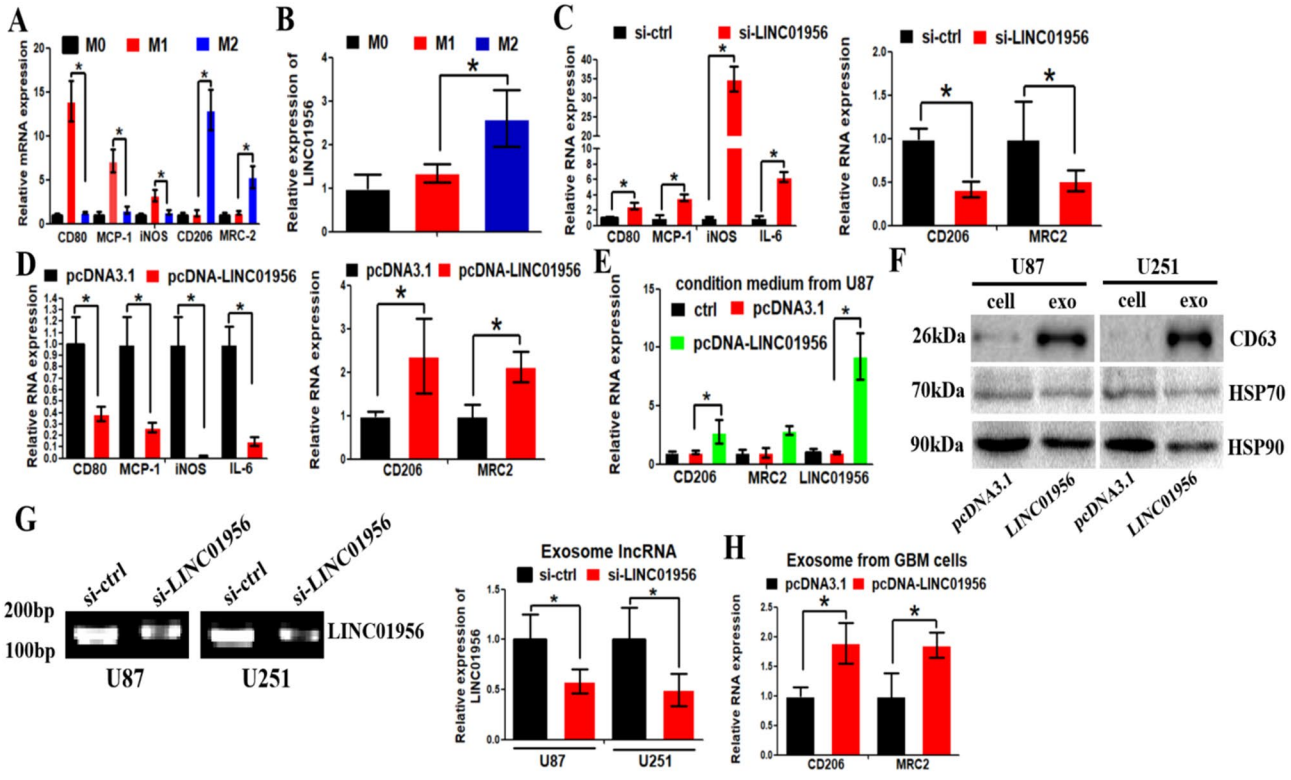

Fig. 8 Exosomal LINC01956 promoted M2 phenotype polarization in GBM cells. (**A**) M1 macrophages-associated genes and M2 macrophages-associated genes were examined by RT-PCR assay. (**B**) LINC01956 expression level was examined in M1 and macrophages, respectively. (**C**) Down-regulation of LINC01956 decreased M2 macrophages markers. (**D**) Over-expression of LINC01956 increased M2 macrophages markers. (**E**) Conditioned medium derived from LINC01956-overexpressing cells increased the expression of M2 markers and LINC01956 in macrophages. (**F**) The western blot assay was used to examine exosome-related proteins. (**G**) Agarose gel electrophoresis and RT-PCR assays were used to detect the expression of LINC01956 in exosomes. (**H**) The expression of M2 markers and LINC01956 in macrophages was examined after culture with the indicated exosomes. *$p < 0.05$. Data are presented as Mean ± SD. One way ANOVA

in the secreted exosomes (Fig. 8G). These data proved the existence of LINC01956 in exosomes. Subsequently, we cocultured unpolarized macrophages with exosomes isolated from pcDNA-LINC01956 control cells. The expression levels of the M2 phenotype markers CD206 and MRC-2 were elevated in the pcDNA-LINC01956 group but not in the control group (Fig. 8H). This finding indicated that exosomal LINC01956 promoted M2 polarization.

Collectively, our findings suggested that LINC01956 could be transferred via exosomes, thereby promoting M2 polarization of macrophages.

LINC01956 was transcriptionally regulated by HIF-1α under hypoxic conditions

Previous studies have demonstrated that a hypoxic TME might contribute to abnormal expression of some lncRNAs, including in GBM. We sought to determine whether LINC01956 was a hypoxia-sensitive lncRNA. We exposed GBM cells to hypoxia or normoxia for 48 h and revealed that HIF-1α and LINC01956 expression levels were elevated (Fig. 9A and B) under hypoxic conditions. The efficiency of HIF-1α downregulation was examined by using western blotting (Fig. 9C). Downregulation of HIF-1α significantly inhibited LINC01956 expression under both normoxic and hypoxic conditions. In addition, downregulation of HIF-1α counteracted hypoxia-induced LINC01956 upregulation(Fig. 9D). We then explored whether HIF-1α regulated LINC01956 by binding to its promoter. Via UCSC and JASPAR bioinformatics software, we analyzed the 1-kb region upstream of the transcription start site of LINC01956 and identified a putative HIF-1α response element (HRE) in the LINC01956 promoter region (positions −367 to -372) (Fig. 9E). To understand whether HIF-1α regulates LINC01956 expression via this HRE, a vector carrying the wild-type LINC01956 promoter and a vector carrying the mutant LINC01956 promoter were constructed. There was an increase in luciferase activity in cells cotransfected with the pcDNA3-HIF-1α plasmid and wild-type LINC01956 promoter. Luciferase activity was impaired in cells that were cotransfected with the pcDNA3-HIF-1α plasmid and mutant LINC01956 promoter (Fig. 9F). Subsequently, the ChIP assay was carried out to confirm that HIF-1α directly bound to the LINC01956 promoter (Fig. 9G). Taken together, our findings implied that LINC01956 was regulated by HIF-1α.

Ailanthone regulated LINC01956 expression via HIF-1α

We performed molecular docking analysis using the database Home for researchers(https://www.dockeasy.cn/). Figure 10A showed the binding model of Ailanthone and HIF-1α, in which the binding sites exhibited good stereocomplementarity. With the use of western blot assay, we found that Ailanthone treatment decreased HIF-1α expression level (Fig. 10B). We observed that Ailanthone treatment decreased LINC01956 expression level, which was counteracted by overexpression of HIF-1α (Fig. 10C).

These data implicated that Ailanthone regulated LINC01956 expression via HIF-1α.

Ailanthone regulated cell growth, invasion and M2 polarization of macrophages via LINC01956

The above findings revealed that Ailanthone regulated LINC01956 expression via HIF-1α, we thus asked whether Ailanthone affected GBM cell growth, invasion and M2 polarization of macrophages via LINC01956.

Our findings revealed that Ailanthone inhibited GBM cell growth, invasion and M2 polarization of macrophages, while overexpression of LINC01956 could counteract these effects (Supplementary Fig. 5A-D).

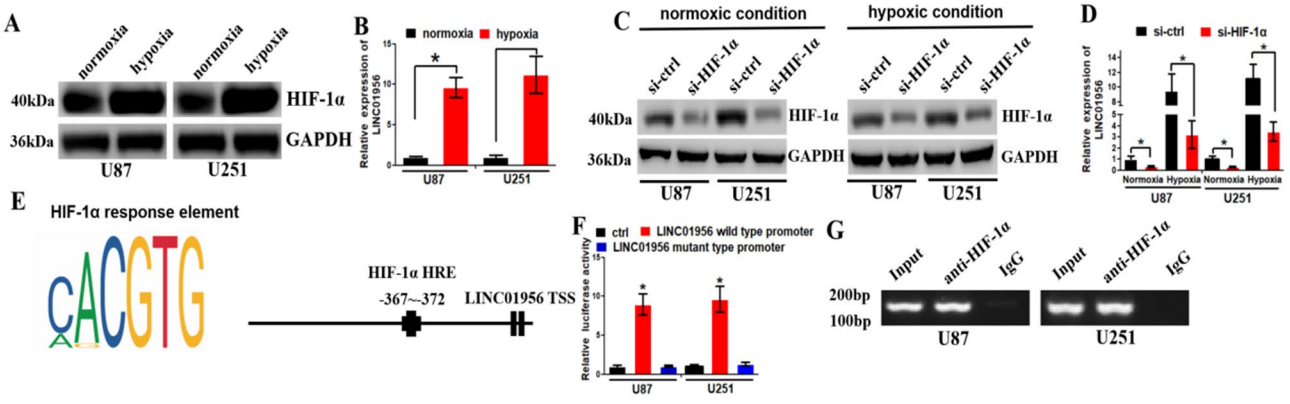

Fig. 9 LINC01956 was transcriptionally regulated by HIF-1α under hypoxic conditions. (**A**) and (**B**) The expression levels of HIF-1α protein or LINC01956 were examined by western blot or RT-PCR assays after culture under normoxia or hypoxia. (**C**) The efficiency of HIF-1α down-regulation was examined by using western blot. (**D**) HIF-1α down-regulation decreased the expression of LINC01956 under normoxia or hypoxia condition. (**E**) The recognition motif of HIF-1α was obtained from the JASPAR database. (**F**) Luciferase activity was examined with the dual-luciferase reporter assay system. (**G**) PCR gel showing amplification of HIF-1α-binding site after ChIP using antibody against HIF-1α. *$p < 0.05$. Data are presented as Mean ± SD. One way ANOVA

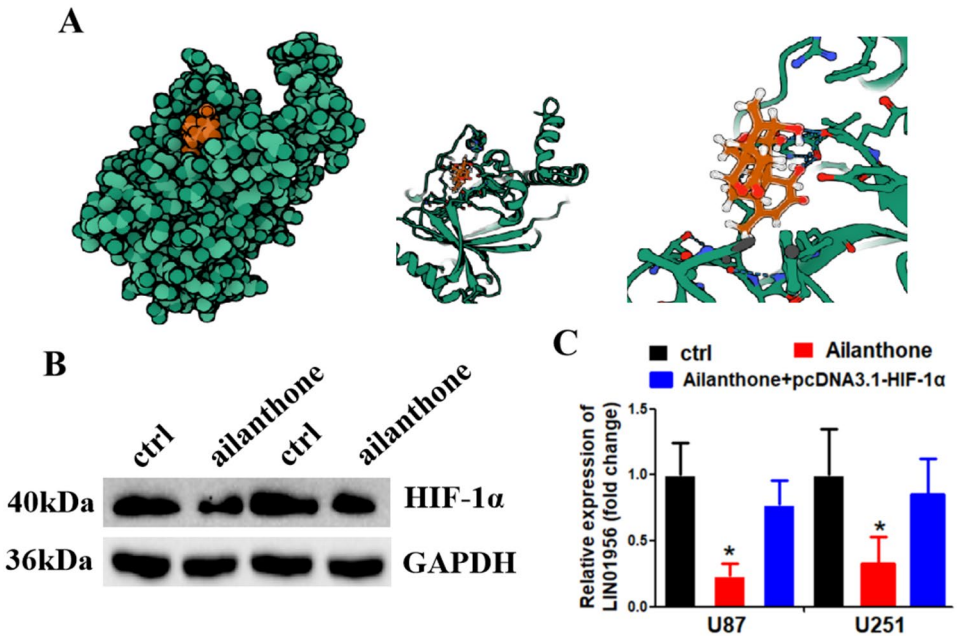

Fig. 10 Ailanthone regulated LINC01956 expression via HIF-1α. (**A**) The most likely predicted targets of Ailanthone in HIF-1α. (**B**) Western blot assay was used to analyze HIF-1α expression level. (**C**) RT-PCR assay was used to analyze LINC01956 expression level. *$p < 0.05$. Data are presented as Mean ± SD. One way ANOVA

Taken together, our data revealed that Ailanthone regulated cell growth, invasion and M2 polarization of macrophages via LINC01956.

Discussion

Recent studies have shown that a growing body of Chinese herbal medicines exhibit significant antitumor properties with minimal adverse effects. Ailanthone is a prominent quassinoid derived from the Chinese botanical species Ailanthus altissima, known for its documented anti-proliferative properties on a variety of cancer cell lines. However, the effect of Ailanthone on TME in GBM is still poorly investigated.

LncRNAs widely participate in regulating the initiation and progression of GBM and are useful diagnostic biomarkers and therapeutic targets for GBM [18, 19]. In our manuscript, we screened for lncRNAs that regulated by Ailanthone in GBM by using lncRNA array. We identified LINC01956 as a lncRNA that was inhibited by Ailanthone in GBM cells. Interestingly, we also found that LINC01956 could be used as a prognostic factor in GBM patients. The biological function assays revealed that downregulation of LINC01956 suppressed cell invasion. These data imply that LINC01956 may be an oncogene in GBM.

The mechanisms by which lncRNAs affect tumorigenesis are complicated [20, 21]. Recently, it was reported that lncRNAs may exert their effects via specific interactions with functional proteins [22]. We thus explored whether LINC01956 exerted its effects by binding with specific proteins. Via the starBase database, we identified FUS, and by using a co-IP assay, we confirmed that LINC01956 directly interacted with FUS. Interestingly, our study elucidated the mechanism of LINC01956 forming a complex with FUS and β-catenin. This effect led to β-catenin nuclear translocation and thus activated Wnt/β-catenin signaling in glioma cells. Abnormal Wnt/β-catenin signaling plays an important role in pathologies, especially in human cancers [23]. Suppression of β-catenin inhibits multiple oncogenic targets in human glioma cells [24]. In the present study, we revealed that downregulation of LINC01956 decreased the activity of Wnt/β-catenin signaling in glioma cells. Our findings suggest that LINC01956 modulates the Wnt/β-catenin signaling pathway and promotes glioma progression.

Recently, studies have focused on the TME, a complex community that includes cancer cells, cancer-associated fibroblasts (CAFs), and immune/inflammatory cells [25]. TAMs, one of the most abundant immune cell populations in various solid cancers, are strongly associated with cancer cell proliferation and metastasis [26]. According to their different biological properties, macrophages can be classified into proinflammatory (M1) and anti-inflammatory (M2)macrophages [27]. TAMs, considered M2-like macrophages, are strongly correlated with cancer progression, including in glioma [28]. Our findings showed that LINC01956 was enriched in M2-like macrophages but not in M1-like macrophages or unpolarized macrophages. In addition, downregulation of LINC01956 significantly decreased the expression

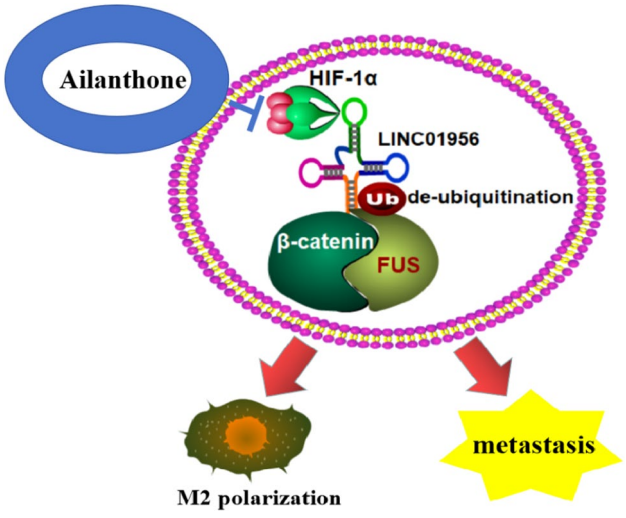

Fig. 11 Ailanthone could be explored as a promising agent in the field of GBM therapy via targeting the HIF-1α/LINC01956/FUS/β-catenin axis

of M2-like macrophage markers. These data imply that LINC01956 is involved in M2 polarization. Interestingly, the supernatant from LINC01956-overexpressing cells contributed to increased expressionof M2 markers, and this finding prompted us to explore the underlying mechanism mediating the communication between glioma cells and macrophages. Previous findings indicated that lncRNAs can be transferred via exosomes to regulate the TME [29]. In parallel, our findings revealed that glioma cell-derived exosomes promoted M2 polarization and thus exerted a tumor-promoting effect by transporting LINC01956.

As a universal phenomenon in a series of cancers, hypoxia is closely associated with cancer progression [30]. Previous studies have revealed that lncRNAs can be regulated by hypoxia via HIF-1α-mediated transcriptional regulation [30]. A series of hypoxia-sensitive lncRNAs have been reported to be involved in tumorigenesis and tumor metastasis [31]. Similarly, we found that LINC01956 was regulated by HIF-1α under hypoxic conditions. Hypoxia elevated the expression level of LINC01956, while this effect was abolished by downregulation of HIF-1α. HIF-1α usually regulates its downstream targets via HREs. Via the JASPAR database, we identified a potential HRE in the promoter region of LINC01956. In addition, we identified the regulatory effect of HIF-1α on LINC01956 transcription by ChIP and dual-luciferase reporter assays. Thus, our findings provide new evidence that supports the idea that LINC01956 acts as a link between hypoxia and glioma progression.

Our data further demonstrated that Ailanthone directly bound to HIF-1α and decreased HIF-1α expression level. Ailanthone regulated LINC01956 expression level via HIF-1α. Finally, we observed that Ailanthone could regulated cell growth, invasion and M2 polarization of macrophages by regulating LINC01956.

Conclusion

Taken together, these data provided a better understanding of Ailanthone in regulating cell growth, invasion and TME in GBM. Our data implied that Ailanthone could be explored as a promising agent in the field of GBM therapy via targeting the HIF-1α/LINC01956/FUS/β-catenin axis (Fig. 11).

Abbreviations

BLI	Biolayer interferometry
CHIP	Chromatin immunoprecipitation
Co-IP	Coimmunoprecipitation
GBM	glioblastoma
IF	Immunofluorescence
lncRNAs	Long noncoding RNAs
PVDF	polyvinylidene fluoride
RIP	RNA immunoprecipitation
RBPs	RNA-binding proteins
TAMs	Tumor-associated macrophages
TCGA	The Cancer Genome Atlas

Author contributions

G. Z. and X.B. D. conceptualized and designed the study. G.Z. wrote the paper draft. X.B. D. corrected the draft. Q.B.Z. helped to revise the manuscript. X.B. D., F.J. and F.F.L. performed the experiments. G.Z. and X.B. D. supervised the experimentators. Z.Y.Y. prepared the dataset. L.W.H., G.S.D. and M.L.Z. analyzed and interpreted the data. All data were generated in-house, and no paper mill was used. All authors agree to be accountable for all aspects of work ensuring integrity and accuracy.

Funding

This work was supported by Four "Batches" Innovation Project of Invigorating Medical through Science and Technology of Shanxi Province (NO. 2023XM055) and Outstanding Youths Project of Shanxi Science and Technology Department (201901D211524).

Data availability

No datasets were generated or analysed during the current study.

Declarations

Ethics approval and consent to participate

This study was approved by the ethical review board of Shanxi Province People's Hospital and Zhujiang Hospital, Southern Medical University. All of the patients were given and accepted informed consent form prior to their enrollment.

Competing interests

The authors declare no competing interests.

Author details

[1]Guangzhou Institute of Cancer Research, the Affiliated Cancer Hospital, Guangzhou Medical University, Guangzhou, China
[2]Cancer Research Institute, School of Basic Medical Sciences, Southern Medical University, Guangzhou, Guangdong, China
[3]The National Key Clinical Specialty, The Engineering Technology Research Center of Education Ministry of China, Guangzhou, China
[4]Guangdong Provincial Key Laboratory on Brain Function Repair and Regeneration Department of Neurosurgery, Zhujiang Hospital, Southern Medical University, Guangzhou, China
[5]The Radiotherapy Department of Shanxi Province People Hospital, Taiyuan, China

Received: 8 July 2024 / Accepted: 28 November 2024

Published online: 05 December 2024

References

1. Reardon DA, Rich JN, Friedman HS, Bigner DD. Recent advances in the treatment of malignant astrocytoma. J Clin Oncology: Official J Am Soc Clin Oncol. 2006;24(8):1253–65.
2. Iwamoto FM, Kreisl TN, Kim L, Duic JP, Butman JA, Albert PS, Fine HA. Phase 2 trial of talampanel, a glutamate receptor inhibitor, for adults with recurrent malignant gliomas. Cancer. 2010;116(7):1776–82.
3. Quinn JJ, Chang HY. Unique features of long non-coding RNA biogenesis and function. Nat Rev Genet. 2016;17(1):47–62.
4. Prensner JR, Chinnaiyan AM. The emergence of lncRNAs in cancer biology. Cancer Discov. 2011;1(5):391–407.
5. Petty AJ, Yang Y. Tumor-associated macrophages: implications in cancer immunotherapy. Immunotherapy. 2017;9(3):289–302.
6. Biswas SK, Gangi L, Paul S, Schioppa T, Saccani A, Sironi M, Bottazzi B, Doni A, Vincenzo B, Pasqualini F, et al. A distinct and unique transcriptional program expressed by tumor-associated macrophages (defective NF-kappaB and enhanced IRF-3/STAT1 activation). Blood. 2006;107(5):2112–22.
7. Huang JK, Ma L, Song WH, Lu BY, Huang YB, Dong HM, Ma XK, Zhu ZZ, Zhou R. LncRNA-MALAT1 promotes angiogenesis of thyroid Cancer by modulating Tumor-Associated Macrophage FGF2 protein secretion. J Cell Biochem. 2017;118(12):4821–30.
8. Han D, Fang Y, Guo Y, Hong W, Tu J, Wei W. The emerging role of long non-coding RNAs in tumor-associated macrophages. J Cancer. 2019;10(26):6738–46.
9. Ma L, Zhang G, Miao XB, Deng XB, Wu Y, Liu Y, Jin ZR, Li XQ, Liu QZ, Sun DX, et al. Cancer stem-like cell properties are regulated by EGFR/AKT/beta-catenin signaling and preferentially inhibited by gefitinib in nasopharyngeal carcinoma. FEBS J. 2013;280(9):2027–41.
10. Li XQ, Yang XL, Zhang G, Wu SP, Deng XB, Xiao SJ, Liu QZ, Yao KT, Xiao GH. Nuclear beta-catenin accumulation is associated with increased expression of nanog protein and predicts poor prognosis of non-small cell lung cancer. J Transl Med. 2013;11:114.
11. Tian X, Wu Y, Yang Y, Wang J, Niu M, Gao S, Qin T, Bao D. Long noncoding RNA LINC00662 promotes M2 macrophage polarization and hepatocellular carcinoma progression via activating Wnt/beta-catenin signaling. Mol Oncol. 2020;14(2):462–83.
12. Mao Q, Min J, Zeng R, Liu H, Li H, Zhang C, Zheng A, Lin J, Liu X, Wu M. Self-assembled traditional Chinese nanomedicine modulating tumor immunosuppressive microenvironment for colorectal cancer immunotherapy. Theranostics. 2022;12(14):6088–105.
13. Liang Y, Song X, Li Y, Chen B, Zhao W, Wang L, Zhang H, Liu Y, Han D, Zhang N, et al. LncRNA BCRT1 promotes breast cancer progression by targeting miR-1303/PTBP3 axis. Mol Cancer. 2020;19(1):85.
14. Ni W, Yao S, Zhou Y, Liu Y, Huang P, Zhou A, Liu J, Che L, Li J. Long noncoding RNA GAS5 inhibits progression of colorectal cancer by interacting with and triggering YAP phosphorylation and degradation and is negatively regulated by the m(6)a reader YTHDF3. Mol Cancer. 2019;18(1):143.
15. Garcia C, Dubois LG, Xavier AL, Geraldo LH, da Fonseca AC, Correia AH, Meirelles F, Ventura G, Romao L, Canedo NH, et al. The orthotopic xenotransplant of human glioblastoma successfully recapitulates glioblastoma-microenvironment interactions in a non-immunosuppressed mouse model. BMC Cancer. 2014;14:923.
16. Yang H, Zhang X, Lu Y, Wang X, Zhang Z, Xu H, Li F, Chen Q, Bai Y, Bai X, et al. Ailanthone induces autophagy and ferroptosis in non–small cell lung cancer Lewis cells. Mol Clin Oncol. 2024;20(3):25.
17. Xue M, Chen W, Xiang A, Wang R, Chen H, Pan J, Pang H, An H, Wang X, Hou H, et al. Hypoxic exosomes facilitate bladder tumor growth and development through transferring long non-coding RNA-UCA1. Mol Cancer. 2017;16(1):143.
18. Liu X, Zhu Q, Guo Y, Xiao Z, Hu L, Xu Q. LncRNA LINC00689 promotes the growth, metastasis and glycolysis of glioma cells by targeting miR-338-3p/PKM2 axis. Biomed Pharmacotherapy = Biomedecine Pharmacotherapie. 2019;117:109069.
19. Yao X, Li X, Luo Y, Xu X, Liu J, Bu J. LncRNA GAS5 regulates Osteosarcoma Cell Proliferation, Migration, and Invasion by regulating RHOB via sponging miR-663a. Cancer Manag Res. 2020;12:8253–61.
20. Li Q, Wu Q, Li Z, Hu Y, Zhou F, Zhai Z, Yue S, Tian H. LncRNA LINC00319 is associated with tumorigenesis and poor prognosis in glioma. Eur J Pharmacol. 2019;861:172556.
21. Du W, Feng Z, Sun Q. LncRNA LINC00319 accelerates ovarian cancer progression through miR-423-5p/NACC1 pathway. Biochem Biophys Res Commun. 2018;507(1–4):198–202.
22. Wang Y, Lu JH, Wu QN, Jin Y, Wang DS, Chen YX, Liu J, Luo XJ, Meng Q, Pu HY, et al. LncRNA LINRIS stabilizes IGF2BP2 and promotes the aerobic glycolysis in colorectal cancer. Mol Cancer. 2019;18(1):174.
23. Bordonaro M, Tewari S, Cicco CE, Atamna W, Lazarova DL. A switch from canonical to noncanonical wnt signaling mediates drug resistance in colon cancer cells. PLoS ONE. 2011;6(11):e27308.
24. He L, Zhou H, Zeng Z, Yao H, Jiang W, Qu H. Wnt/beta-catenin signaling cascade: a promising target for glioma therapy. J Cell Physiol. 2019;234(3):2217–28.
25. Hinshaw DC, Shevde LA. The Tumor Microenvironment innately modulates Cancer Progression. Cancer Res. 2019;79(18):4557–66.
26. Dymicka-Piekarska V, Koper-Lenkiewicz OM, Zinczuk J, Kratz E, Kaminska J. Inflammatory cell-associated tumors. Not only macrophages (TAMs), fibroblasts (TAFs) and neutrophils (TANs) can infiltrate the tumor microenvironment. The unique role of tumor associated platelets (TAPs). Cancer Immunol Immunotherapy: CII. 2021;70(6):1497–510.
27. Kim J, Bae JS. Tumor-Associated Macrophages and Neutrophils in Tumor Microenvironment. Mediators of inflammation 2016, 2016:6058147.
28. Komohara Y, Fujiwara Y, Ohnishi K, Takeya M. Tumor-associated macrophages: potential therapeutic targets for anti-cancer therapy. Adv Drug Deliv Rev. 2016;99(Pt B):180–5.
29. Xiao M, Zhang J, Chen W, Chen W. M1-like tumor-associated macrophages activated by exosome-transferred THBS1 promote malignant migration in oral squamous cell carcinoma. J Experimental Clin cancer Research: CR. 2018;37(1):143.
30. Henze AT, Mazzone M. The impact of hypoxia on tumor-associated macrophages. J Clin Investig. 2016;126(10):3672–9.
31. Hua Q, Mi B, Xu F, Wen J, Zhao L, Liu J, Huang G. Hypoxia-induced lncRNA-AC020978 promotes proliferation and glycolytic metabolism of non-small cell lung cancer by regulating PKM2/HIF-1alpha axis. Theranostics. 2020;10(11):4762–78.

Publisher's note